

# Simulation of Satellite Interactions with Solar Flares Using Analysis System (ANSYS) Software

Anetor J. Ighodalo<sup>1</sup>, Yusuf S. I.<sup>2\*</sup>, Dada O. Michael<sup>1\*</sup>

<sup>1</sup>Department of Physics, Federal University of Technology, PMB 65, Minna, Niger State

<sup>2</sup>Department of Mathematics, Federal University of Technology, PMB 65, Minna, Niger State

\*Corresponding authors: shakirudeen.yusuf@futminna.edu.ng, dadamichael@futminna.edu.ng

## Abstract

Solar flares produce high-energy particles and radiation that are dangerous to living organisms. The x-rays from flares are stopped by our atmosphere well above the Earth's surface. However, they do disturb the Earth's ionosphere, which in turn disturbs some radio communications. Along with energetic ultraviolet radiation, they heat the Earth's outer atmosphere, causing it to expand. This increases the drag on Earth-orbiting satellites, reducing their lifetime in orbit. Furthermore, these atmosphere changes and intense radio emission from flares can degrade the precision of Global Positioning System (GPS) measurements. Hence, computer simulation of these interactions is very important for improved satellite designs. In this study, the use of magnetic fields to deflect energetic charged particles has been proposed as a means of simulating the interaction of satellites from the harmful radiation encountered in space. These so-called active magnetic shields must provide a region of space, which is protected from energetic particles below a given energy while also maintaining a safe level of magnetic field strength within the shielded region. Toroidally shaped environments with circular coils of wire distributed on the surface of the spacecraft have been used to mimic this condition with ANSYS software. Numerical techniques have been employed to demonstrate that particles below a given energy, including galactic cosmic rays (GCRs) are completely shielded from a region inside the toroidal spacecraft. Appropriate amplitudes of the currents flowing in the circular coils were chosen while the magnetic field-strength inside this region were made to be arbitrarily small within the toroidal spacecraft. While many practical issues must be addressed with this computational design, this study has been able to demonstrate the possibility of constructing a magnetic field suitable for protecting satellites from GCRs during long-duration manned missions.

**Keywords:** Solar flares, Earth-orbiting satellites, Global Positioning System, ANSYS, Numerical simulation.

## Introduction

Recent technological advances have allowed man to expand beyond the near earth environment into a new frontier. This expansion is accomplished through the launching of satellites into various earth orbits. The more satellites we launch, the more we learn about the space environment surrounding Earth. Unfortunately, the space environment has proven to be hostile to satellites and has resulted in large amounts of research being directed to determine both the causes and remedies for these hostilities. One of the areas receiving attention is in the unexpected satellite anomalies (Wong, 1991).

Satellites operating in these hostile environments interact with elements such as cosmic rays, energetic protons, plasma and solar flares. Studies have confirmed that adverse interaction can cause on-orbit anomalies and can lead to serious consequences to the operation of satellites in space (Wong, 1991).

Solar flares are magnetically driven explosions on the surface of the sun, which are interpreted as a large energy release of up to  $6 \times 10^{25}$  joule of energy. They are mainly followed by a colossal coronal mass ejection also known as a CME

([http://en.wikipedia.org/wiki/Solar\\_flare](http://en.wikipedia.org/wiki/Solar_flare)). The flare ejects clouds of electrons, ions, and atoms through the corona of the sun into space ([http://en.wikipedia.org/wiki/Solar\\_flare](http://en.wikipedia.org/wiki/Solar_flare)).

Approximately 8 minutes after a solar flare occurs on the surface of the sun, a powerful burst of electromagnetic radiation in the form of X-ray, extreme ultraviolet rays, gamma ray radiation and radio burst arrives at Earth (Marusek, 2007). The ultraviolet rays heat the upper atmosphere which causes the outer atmospheric shell to expand. The x-rays strip electrons from the atom in the ionosphere producing a sudden increase in total electron content (Marusek, 2007).



Figure 1: Solar Flares (<http://www.mnn.com/earth-matters/space/stories/solar-flare-could-disrupt-earth-s-satellite-communications>)

There are typically three stages to a solar flare. First is the precursor stage, where the release of magnetic energy is triggered. Soft x-ray emission is detected in this stage. In the second or impulsive stage, protons and electrons are accelerated to energies exceeding 1 MeV. During the impulsive stage, radio waves, hard x-rays, and gamma rays are emitted. The gradual build up and decay of soft x-rays can be detected in the third, decay stage. The duration of these stages can be as short as a few seconds or

as long as an hour (<http://hesperia.gsfc.nasa.gov/sftheory/flare.htm>).

These flares can be classified according to their brightness in the x-ray wavelength. They group flares into 3 categories (X-class, M-class and C-class). In Table 1, C-class flares are very small and produce few noticeable effects on Earth. M-class flares are medium-size and can cause brief radio blackouts in the Polar Regions. X-class flares are major events that can trigger worldwide radio blackouts and radiation storms in the upper Atmosphere (Marusek, 2007).

The sun undergoes a cyclical ( $\approx 22$  years) pattern of magnetic pole reversals observable in the frequency of sunspot activity. This pattern is comprised of two  $\approx$  eleven year cycles phases. In the first phase, the sun's magnetic poles reverse polarity. In the second phase, the sun reverses the magnetic polarity again the pole back to its original polarity. Solar storm activity is strongly phase dependent and also very dependent on the position within the solar cycle (Marusek, 2007).

Sunspots are the site of origin for great solar storms while the sun spins on its axis. As seen from earth, the average rotation period of the Sun averages 27 days. Great sunspot groups can stay active for several solar revolutions creating a cyclical  $\sim 27$  day pattern of solar storms.

Solar storms vary in size and impact on Earth. One of the largest solar storms in the past 450 years occurred in September 1859. The Sun Kings by Stuart Clark is an excellent book describing this particular solar storm, known as the Carrington flare. Because our civilization has evolved into a technologically driven /technology dependent

society, a solar storm of this magnitude today could produce a major global calamity.

This analysis is primarily focused on the rare massive solar storms that occur at a rate measured in terms of decades and centuries. There is an element of danger to these great storms and without an adequate assessment, one might be caught unawares or blindsided to this very real threat (Marusek, 2007). It has been established that 'space weather changes' is due to solar activity and can impact infrastructural systems (Harsh and Ananna, 2012). CME can cause geomagnetic storms which are capable of affecting many systems. Recent US FERC, EMP commissions have noted that most power grids are potentially most severely affected infrastructures. Its effect will surely be there on communication systems as well (Harsh and Ananna, 2012). In present scenario there is also a possibility that in uneasy circumstances if a missile is fired from one country to other country then electromagnetic pulses generated from above causes can detonate the nuclear weapon. E1 EMP and international electromagnetic interface can also damage control systems.

Geomagnetic storms can be referred to as magnetic disturbances in the earth's otherwise normal geo magnetic field. In present circumstances the effect on power grids can hamper the communication systems, thus halting the life and causing huge monetary damages. Even if point of devastation is not brought, the effect on communication lines and disruption in communication is not just a real possibility but also a prejudice.

Geomagnetic storms and their impacts on power grids have been widely studied. Its impact on North American power grids occurs at disturbances of around 500nT/minutes. Whereas the magnitude of effect in 1972 was greater than 2000nT/minutes. The disturbances on 14 May, 1921 is considered as largest storm of the previous century and according to present estimate, these storms can be anywhere between 4 to 10 times more than the observed ones. Geomagnetic storm if of large severity will have larger planetary footprint. It has been estimated that geomagnetic induced current (GIC) are possible at low latitudes (Harsh and Ananna, 2012). The ring current and ground level disturbances were observed on 15 July, 2000. In Japan on 6 Nov, 2001 the GIS flows in the network were observed.

In November, 2003, five major stations, 15 large transformers, encountered an unknown storm which led to the collapse. It is estimated that GIS activated the above storm. Going by this theory, we can state that larger storms will have higher impact on power grids and communication lines (Harsh and Ananna, 2012). Great solar storms occur approximately once per decade. Table 1.1 lists the great solar storms over the past 150 years.

The largest observed solar flare was the Carrington white light flare of September 1, 1859. The largest measured solar flare occurred on November 4, 2003 and was rated as an X45. Fortunately, this flare only grazed Earth but not the satellites. Solar flares produce satellite communications interference, radar interference, shortwave radio fades and blackout and atmospheric drag on satellite producing an unplanned change in orbit.

*Dst* is an abbreviation for the Disturbance Storm Time index that measures the strength of the magnetic storm by averaging the horizontal components of the geomagnetic field

Date	Solar Flare Intensity	Omni-Directional Solar Proton Fluence	Main CME Arrival Time	Magnetic Intensity Disturbance Storm Time (Dst) (nano-Teslas)
1-2 September 1859	Sept 1 Carrington White Light Flare	$1.88 \times 10^{10} \text{ cm}^{-2}$	17 hours 40 mins	Sept 2 - 1,760 nT ( $\Delta H$ at Bombay 1,720 nT)
12 October 1859				( $\Delta H$ at Bombay 980 nT)
4 February 1872				( $\Delta H$ at Bombay 1,020 nT)
17-18 November 1882				( $\Delta H$ at Greenwich > 1,090 nT)
30 March 1894		$1.11 \times 10^{10} \text{ cm}^{-2}$		
31 October 1903				( $\Delta H$ at Potsdam > 950 nT)
25 September 1909				( $\Delta H$ at Potsdam > 1,500 nT)
13-16 May 1921				( $\Delta H$ at Potsdam 1,060 nT)
7 July 1928				( $\Delta H$ at Alibag 780 nT)
16 April 1938				( $\Delta H$ at Potsdam 1,900 nT)
13 September 1957				Sept 13 - 427 nT
11 February 1958				Feb 11 - 426 nT
13 March 1989	X15			Mar 13/14 - 589 nT
29 October - 5 November 2003	Oct 28 X17.2 Oct 29 X10 Nov 4 X45		19 hours	Oct 29 -353 nT Oct 30 -383 nT Nov 5 (missed Earth)
18-21 November 2003	Nov 18 M3.2			Nov 20/21 - 422 nT

Table 1: Great Solar Storm (Marusek, 2007)

Class	Peak Flux(W/m <sup>2</sup> ) 100-800 picometer x-rays near the Earth	Class	Peak Flux(W/m <sup>2</sup> ) 100-800 picometer x-rays near the Earth
X1	$1.0 \times 10^{-4}$	M1	$0.1 \times 10^{-4}$
X2	$2.0 \times 10^{-4}$	M2	$0.2 \times 10^{-4}$
X3	$3.0 \times 10^{-4}$	M3	$0.3 \times 10^{-4}$
X4	$4.0 \times 10^{-4}$	M4	$0.4 \times 10^{-4}$
X5	$5.0 \times 10^{-4}$	M5	$0.5 \times 10^{-4}$
X6	$6.0 \times 10^{-4}$	M6	$0.6 \times 10^{-4}$
X7	$7.0 \times 10^{-4}$	M7	$0.7 \times 10^{-4}$
X8	$8.0 \times 10^{-4}$	M8	$0.8 \times 10^{-4}$
X9	$9.0 \times 10^{-4}$	M9	$0.9 \times 10^{-4}$

Table 2: Classification of Solar Flare Intensity (Marusek, 2007)

Scientists at NASA have been warning for sometime of the dangers of space weather affecting the Earth and particularly the danger of solar storms. With the sun due to reach the top of both its 22-year magnetic energy circle and 11-year Sunspot circle in 2013, there is real danger of magnetic

energy damaging electronic equipments (<http://www.wired.co.uk/news/archive/2010-06/15/how-to-survive-a-solar-storm>).

Solar events happen all the time, but 2013 is predicted to be a particularly bad year due to the peaking of several sun cycles. The last time this

happened was in 1859 when the largest recorded solar storm spun compasses, disrupted telegraph service, and lit up the skies. Our dependency on electronics and an overloaded power grid makes us much more vulnerable to solar storms today.

These “solar storms” bombard the solar system – and Earth – with radiation and magnetic shock waves that can wreak havoc on magnetic fields, power systems, and electronics devices. The Earth’s atmosphere shields us from much of the radiation, but solar storms can still do quite a bit of damage, including:

- i. Short out satellites and take down GPS, cell phones, Internet, and TV services
- ii. Cause damage to electronic devices and computers
- iii. Disrupt the power grid resulting in overloads, widespread power outages, and dangerous power surges

## **Methods**

The study of fluid has been around for millennium, dating back to ancient Greece, but their understanding did not go beyond what they needed to know to run aqueducts and other waterworks. Da Vinci further pursued the topic during the Renaissance observing waves and free jets. Even Newton studied fluids. The topic did not mature until people like Bernoulli and Euler investigated it and developed equations that were later named after them. The Euler equations were further modified by Claude Louis Marie Henry Navier and George Gabriel Stokes to create the Navier-Stokes equation. These men laid the groundwork that would be the foundation of computational fluid dynamics.

- iv. Knock out radio communications and military communications.

The purpose of this research is to simulate how an orbiting satellite will shield solar flares using ANSYS Software. The objectives of this research are to (1) simulate solar flares using fluid flow (fluent) in ANSYS Software (2) solve using the governing equations in fluent (3) use fluent to create an animation of solar flares been shielded by a satellite

This study mainly focused on the reinforcement of a communication satellite with a detector that senses the magnetic radiation of the sun and be able to repel or shield this radiation from affecting the on-board components of the satellite. The study was carried out by using ANSYS software. Simulation was run by using FLUID FLOW FLUENT, a module in ANSYS software.

Computational fluid dynamics is a term used to describe a way of modeling fluids using algorithms and numerical methods. Currently they are solved utilizing computers but early methods were completed manually without the aid of a computer. Computational fluid dynamics are a powerful tool to model fluids, but even with the most state of the art supercomputers and technological advances they are only an approximation of what would occur in reality.

It is unclear exactly when computational fluid dynamics came into being. Lewis Fry Richardson attempted to predict the weather by creating a grid in physical space and using Bjerknes's "primitive

differential equations". His method involved a stadium of 64,000 people each using a mechanical calculator to solve part of the flow equation. It ended in failure. In 1933, A. Thom was able to numerically compute flow past a cylinder. Another mechanical solution was made by M. Kawaguti which took 20 hours a week over 18 months. NASA's theoretical division also made contributions during the 1960s, but it wasn't until the 1980s when commercial methods for computational fluid dynamics became available (<http://www.wpi.edu/Pubs/E-project/Available/E-project121509172041/unrestricted/mqp.pdf>).

CFD stands for computational fluid dynamics. It is a way of modeling complex fluid flow by breaking down geometry into cells that comprise a mesh. At each cell an algorithm is applied to compute the

fluid flow for the individual cell. Depending on the nature of the flow either the Euler or Navier-Stokes equations can be used for the computation.

It is very important to discuss GAMBIT before explaining what fluent is. GAMBIT (Figure 2.1) is an application that is distributed along with FLUENT. As of this writing, it is owned and distributed by ANSYS, Inc. GAMBIT is used as a tool to generate or import geometry so that it can be used as a basis for simulations run in FLUENT. It can either build a model or import existing geometries from various other CAD applications. With geometry in place it generates a mesh for the surface and volume of the geometry allowing it to be used for computational fluid dynamics (<http://www.wpi.edu/Pubs/E-project/Available/E-project121509172041/unrestricted/mqp.pdf>).

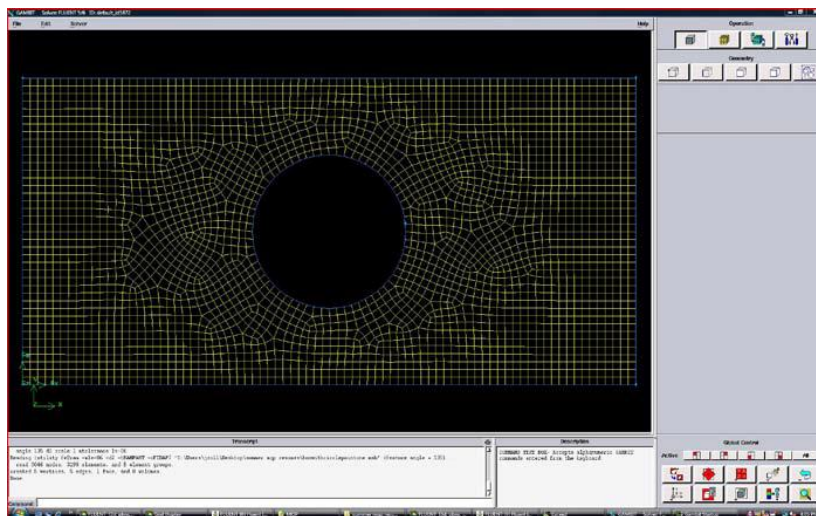


Figure 2: Gambit 2.4.6 General User Interface

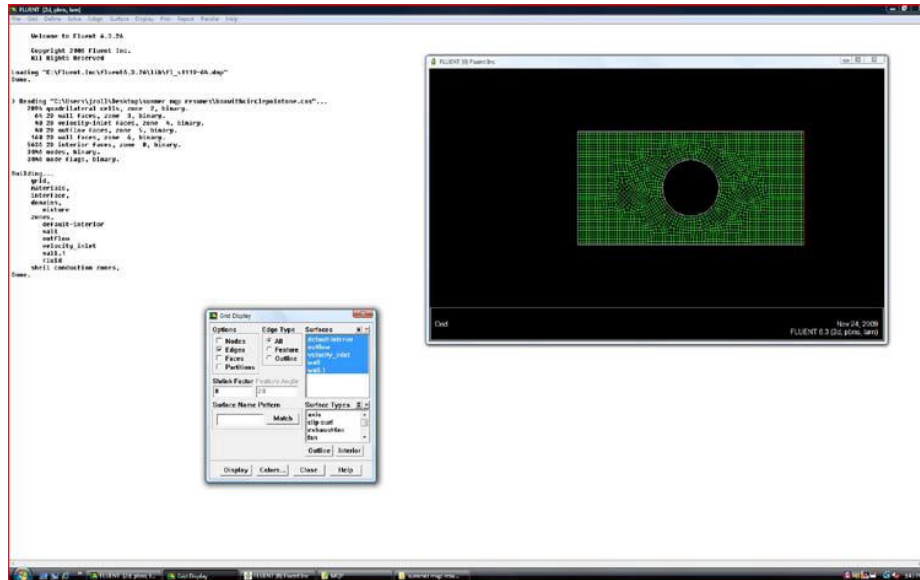


Figure 3: Fluent 6.3.26 General User Interface

FLUENT (as shown in Figure 3) is a “Flow Modeling Software” owned by and distributed by ANSYS, Inc. It is used to model fluid flow within a defined geometry using the principles of computational fluid dynamics. Unlike GAMBIT, which it is shipped with, it utilizes a multi window pane system for displaying various configuration menus and grids instead of a single window with several embedded sub-windows restricted within the space of the parent window. FLUENT is able to read geometries generated in GAMBIT and model fluid flow within them. It can model various scenarios using computational fluid dynamics, including compressible and incompressible flow, multiphase flow, combustion, and heat transfer.

*Generating a Simple 2-dimensional Model with a Single Circle in the Center*

In order to generate the model to be simulated, first one must open up GAMBIT. The geometry can either be imported from another source or built within the program. In this test the geometry was

created within GAMBIT. Then solver was selected and Fluent 5/6 chosen. This configures the program to generate a file that will be compatible with the version of FLUENT being used. Next go to Geometry, select Face, and then select Create Face. Since the geometry is rather simple, composed of a circle within a rectangle, there was no need to create the vertexes individually. First, a rectangle with an x-value of 8 and a-y value of 4 and a circle with a radius of 1 were created. Both objects will be created with their center being the origin (Figure 4). In order to place the objects fully within the first quadrant the move command was used. Since they are halfway in both the positive x-axis and y-axis they must be moved in the x-direction and in the y-direction. Next the two geometries need to be consolidated into one. This was done by using the subtract command where one must select the rectangle and subtract the circle from it. After the operation is completed only one face appeared up in the menu.

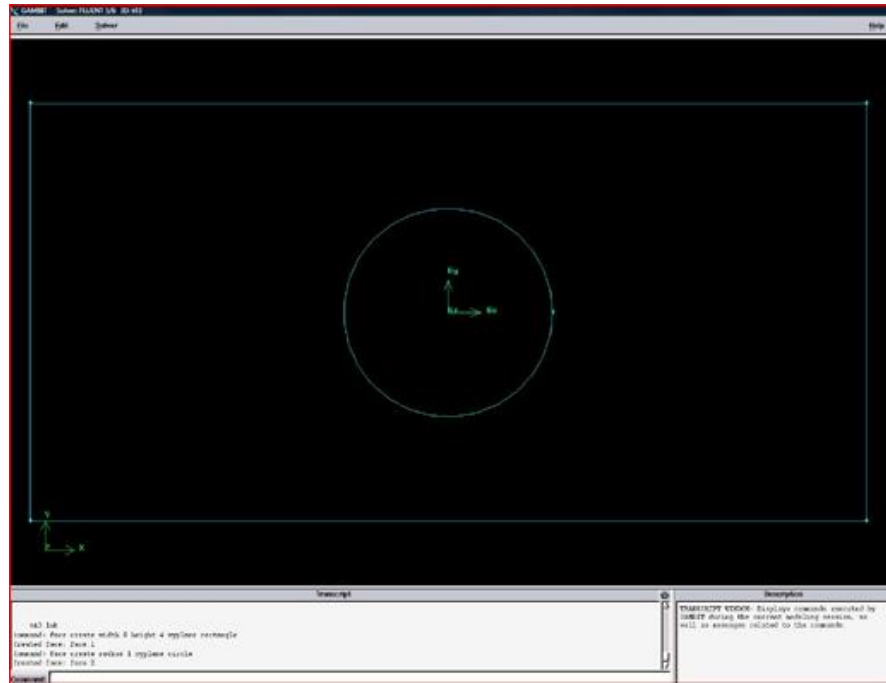


Figure 4: Rectangle and Circle Generated at Origin.

With the geometry created, it was now time to generate a mesh. Mesh was selected, then face, and finally mesh faces. Leave the defaults except for the spacing. Spacing determines how far node points are away from each other and consequently how many are created. The spacing was done in the same units as the geometry used. At the default spacing of 1, a single node is created for every unit of 1. For a side that measures at 4 there would be 4 node

points. Desired spacing was inputted to get the optimal resolution. For the first preliminary tests spacing of 0.5, 0.25, and 0.1 were used, but later tests used 0.1, 0.05, and 0.01. After the mesh was exported, replace the spacing for the mesh with a different one if the resolution isn't accurate enough. When the mesh was generated it looked like a grid that changes shape as it becomes closer to the circle (Figure 5).

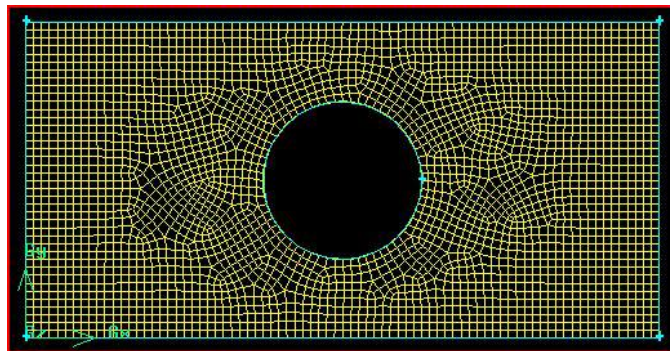


Figure 5: Mesh generated at 0.01 resolution



Next the boundary types needed to be defined. Not every wall of the geometry serves the same purpose, so it was important to determine how Fluent was going to interpret them. For example in this geometry water needs to enter from the left and exit through the right while going around the circle in the middle. On its own Fluent can't determine that is what the user wants, so at this point, inlets, outflows, and walls need to be defined. In order to do this, Zones was selected, likewise the Boundary Types (Figure 2.5). From the drop down menu, left edge was selected. This can be determined by selecting an edge and clicking the arrow that

points to the right which will move the label to the right options list. The edge will be highlighted on the geometry. When the correct edge was selected, click on the Entity drop down menu and select velocity inlet. The edge velocity inlet was labeled for further reference. The steps were repeated for the right edge which was the outflow. The two remaining walls of the rectangle were designated and labeled as wall. Lastly the inner circle should be defined as a wall, but it was labeled circle so it could be accessed separately from the other walls.

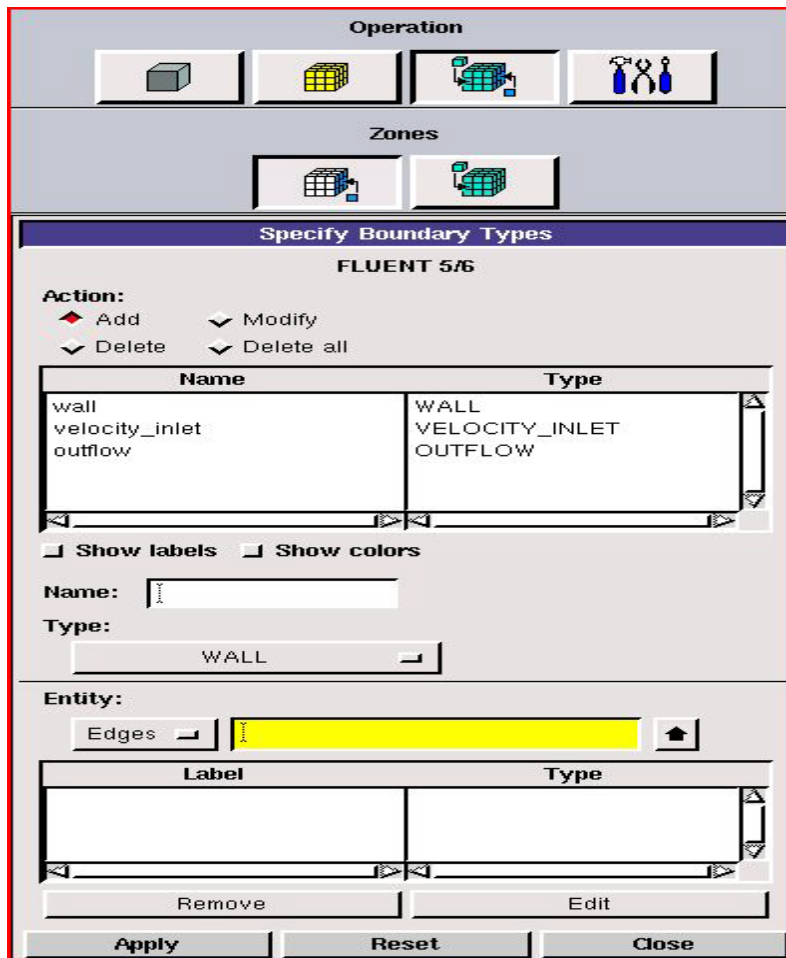


Figure 6: Boundary Types Menu

This was important when reading the forces acting on different elements of the geometry. Now that the mesh has been generated and the boundary types defined, the file was saved and exported as a mesh with the 2D option selected as the model is only utilizing the x and y dimensions.

The file was then opened in Fluent. It presented a list of options, 2d, 2ddp, 3d, and 3ddp. 2d was selected since the geometry generated in GAMBIT was 2-dimensional. Next, File was clicked, Read and then Case in order to import the file from GAMBIT, which ended with a .msh file extension. Before doing anything else in Fluent checks that there were no errors in the geometry. This was done by selecting Grid then Check. Although it was not essential to do this step, doing so will prevent one from running a simulation on faulty geometry, which, considering the nature of how the program uses memory, may cause the program to lock up and the computer to run rather slow as it prints out a series of error messages. Please note that this

did not catch all possible mistakes. Select Display the Grid. A new configuration window asking for criteria to be determined opened up but the defaults were all that was needed, so just select Display. This opened up a new window displaying the model created in GAMBIT. From this point the fluid needed to be defined. This is done by opening up the Materials window (Figure 7) which is located in the Define menu. By default Air is listed, but in this test water was used instead. Water was added by clicking on the Database button. Another configuration window opened up, which listed various materials. Scrolling down to the bottom and selecting Water give two entries for water so of the two pick the one indicating liquid instead of vapor. After clicking Copy and water appeared in the main materials window. In some of the tests the viscosity of Water was changed from the default. For these tests the viscosity value was changed by typing in a new value and clicking Change/Create.

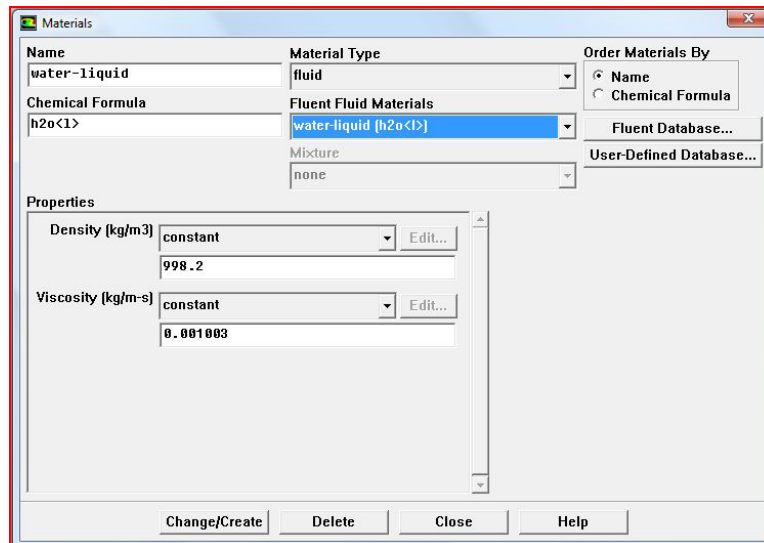


Figure 7: Materials Window

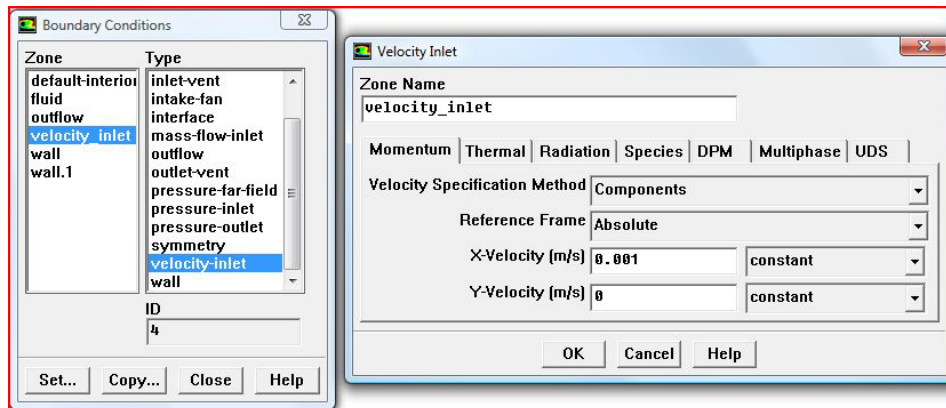


Figure 8: Boundary Conditions and Velocity Inlet Windows

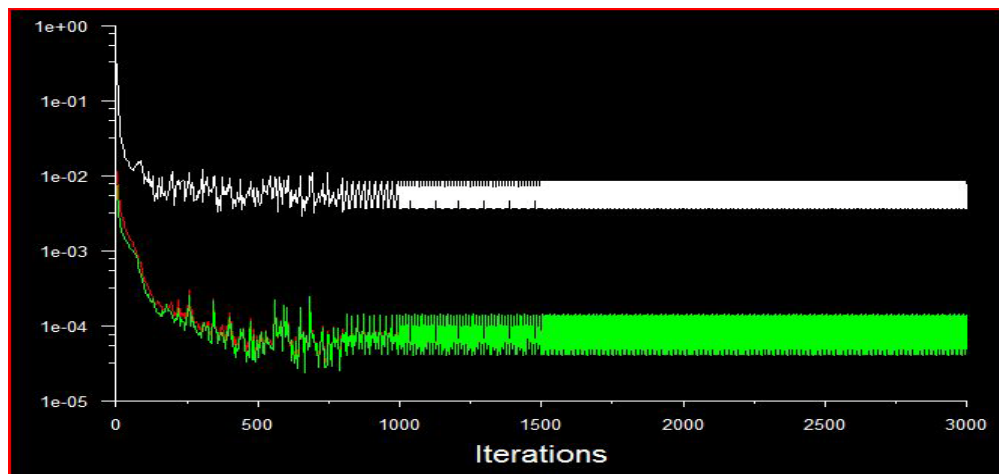


Figure 9: Sample of 3000 Iterations

After defining the materials the boundary conditions needed to be defined. Open the menu by clicking Define and then Boundary Conditions. Then, select fluid in the Zone list and then fluid in the Type list before pressing the Set... button on the bottom. In the drop down menu that says 'air', select it and changed it to water. This tells Fluent that it will use water as the fluid for the simulation. click okay and exit out of the sub window. At this point, return to the Materials window and delete air from the list of available materials so that there won't be any confusion, but this was not necessary. Go to Boundary Conditions window (Figure 2.7) and select the item velocity inlet in both panes and pressed set... again. For the Velocity Specification Method, change from the default option in the drop down menu to Components then change the X-Velocity to 0.001 as that value was be used in this test. Then press OK and exit out of the Boundary Conditions window.

At this point the solution needs to be initialized. To do this go to the Solve menu, pressed Initialization and then initialize, which opened up a window titled Solution Initialization. In the new window click on the drop down menu and select velocity inlet as where it will compute from. For the X Velocity the same number used before which was 0.001 m/s was inputted. Then click Initialize and closed the window.

At this point all conditions were satisfied to run the simulation. From the Solve menu click Monitors and then Residual. This window set the parameters of the simulation. For this test the default options were left alone. Check the radio button next to the Plot option then press OK. In order to run the simulation click Solve then Iterate to open the Iterate window. For number of iterations, type 1000 and then pressed Iterate. The second window that displayed the geometry was replaced with a plot with new points being added as time went. The number of iterations were also be tracked in the main window.

Depending on the resolution running the solution varied in terms of length (Figure 2.8). In a few circumstances the simulation may ended before it could finish all 1000 iterations. This meant the solution had converged and the main window indicated that convergence had been found. In some tests it stopped computing the solution before convergence was found because the computer ran out of memory to run the operation. In other tests the solution did not converge after 1000, which prompted me to go back and run further iterations to see if it converged with more. In the case that they still did not converge, the earlier solution with the one generated after further iterations was compared. After comparing the two, it was determined whether or not they are close enough to pick a solution.

The set of equations characterizing magnetic field or flux are known as the Lorentz force equations. Due to a limited number of known analytical solutions, numerical solvers have been created to provide approximate solutions for magnetic field described by these equations.

The strategy in obtaining a solution of the magnetic field by approximation, usually includes the following five steps: (i) Development of a mathematical model to describe the magnetic field (ii) Discretise the continuous flow domain into a finite number of elements (iii) Decide on an approximate version of the governing equations for each element at any given moment in time (iv) Reduce the number of unknowns by further approximation to obtain a closed system of equations (v) Assemble the system of equations, one system for each element, so that time integration is possible (vi) Solve the equations (vii) Present the results.

In the present study the commercial code Fluent 13.0 by ANSYS has been chosen as the numerical solver. Within Fluent, a laminar model has been selected.

### *Magnetic Field Design*

The magnetic shield works by deflecting the incident charged particle radiation in a magnetic field. For a field  $\vec{B}$ , a particle of charge  $q$  moving with velocity  $\vec{v}$  will be subject to the Lorentz force

$$\vec{F} = \frac{q(\vec{v} \times \vec{B})}{c} = \frac{qvB \sin \theta}{c} \quad (1)$$

where  $\theta$  is the angle between the particle's velocity and the magnetic field. The Lorentz force

always acts perpendicularly to the particle's direction of motion, causing the particle to travel along a curve. In the special case of a relativistic particle with Lorentz factor  $\gamma$  moving perpendicularly to a magnetic field, the trajectory will be circular with radius

$$\rho = \frac{m\gamma v}{\kappa B} \quad (2)$$

where  $\kappa = 0.3 \text{ GeV}/T - m$  (Hoffman *et al.*, 2005). The idea for magnetic shielding of a satellite relies on a toroidal magnetic field surrounding the electronic components volume and oval coils arranged circularly around the electronic components compartment create the field, which is oriented circularly around the axis of the compartment. Charged particles incident from outside the shield will then always have some component of their velocity perpendicular to the magnetic field and will thus be subject to the Lorentz force (Hoffman *et al.*, 2005).

### *Magnetic Shielding Fundamentals*

Charge particles in a strong magnetic field are magnetized and follow adiabatic trajectories under the Lorentz force, which are strictly normal to the velocity vector in the absence of other fields, e.g. electric field:

$$\frac{d\vec{p}}{dt} = q \frac{\vec{v} \times \vec{B}}{c} \quad (3)$$

Here momentum and velocity are linked through the equality  $p = m_0 \gamma v$  with the relativistic factor defined as:

$$\gamma = \sqrt{1 + \left( \frac{p^2}{m_0^2 c^2} \right)} \quad (4)$$

where  $c$  is the speed of light in vacuum;  $m_o$  is the rest mass of the particle;  $p$  is the momentum.

A gyro-frequency of a particle placed in a uniform magnetic field is given by:

$$\omega_H = \frac{qB}{m_o \gamma c} \quad (5)$$

and a corresponding gyro-radius given by:

$$r_H = \left( \frac{v}{\omega_H} \right) = \left( \frac{vm_o \gamma c}{qB} \right) = \left( \frac{pc}{qB} \right) \quad (6)$$

For the ultra-relativistic particles with high energies  $E \gg E_o \equiv m_o c^2$  the product of momentum times speed of light becomes increasingly close to the energy:

$$pc = \sqrt{E^2 - m_o^2 c^4} \rightarrow E \quad (7)$$

and therefore,

$$r_H \rightarrow \left( \frac{E}{qB} \right). \quad (8)$$

In the common used units  $-GeV$  for energy  $E$ , Tesla for magnetic field, and if we measure dimensionless charge in units of electron charge  $q/e=n$ , the Larmor radius in meters reads as

$$r_H(m) \approx 3.336 \frac{E(GeV)}{nB(T)}. \quad (9)$$

Finally, we arrive at a simple estimate of the required "magnetic thickness" of a shield stretching from point A to B that will reflect back all (ultra-relativistic and not) particles with energies equal or smaller than  $E$  regardless of their charge number:

$$E(GeV) < 0.3 \int_A^B B(T) dl(m) = 0.3 < B > \Delta \quad (10)$$

where we integrate along line A-B,  $\Delta$  is the width of the magnetic layer carrying mean magnetic

induction  $\langle B \rangle$ . Of course, particles which layer are not ultra-relativistic will require weaker magnetic insulation. However, quantitative calculations of required thickness have to take into account processes that can change the speed of particles (not to be done numerically, as purely theoretical analysis is limited due to the complexity of the system. We started with the model of the targeted magnetic shield as presented in Fig. 3.1. The coils are assembled in a double-toroidal-solenoid configuration to repel particles coming from all directions and to create a sufficient large inner habitat with vanishing magnetic field (Hoffman *et al.*, 2005).

By choosing

$$\langle B \rangle = 5 - 7T \quad (11)$$

and coil width

$$\Delta = 1 - 2m \quad (12)$$

we can estimate that the cosmic ray spectrum can be significantly reduced at energies up to

$$E < 1.5 - 4.2 GeV. \quad (13)$$

These numbers imply a 70-90% reduction of the cosmic ray flux within the satellite. To reduce penetrating flux to 1% of the nominal intensity, one has to achieve magnetic thickness on the order of  $\approx 30Tm$ .

Next, we estimate currents  $I$  in the coils and magnetic forces  $F$  acting on them. Selecting the target number of coils to be  $K=16$ , and the large radius of the torus  $R \approx 4 - 5m$ .

A mean field inside a toroidal solenoid of major radius  $R$  is given by the expression:

$$B = \frac{\mu_o NI}{2\pi R} = 2 \times 10^{-7} \frac{KI(A)}{R(m)} \quad (14)$$

By substituting input parameter, we estimate that to achieve 30Tm, the required current has to be substantial,  $I \approx 10MA$ . The forces acting on coils could be estimated as follows. The magnetic force per unit length acting on two parallel currents  $I$  separated by distance  $\Delta$  is given by formula:

$$F(Nm^{-1}) = \frac{\mu_o I^2}{2\pi\Delta} = 2 \times 10^{-7} \frac{I^2(A)}{\Delta(m)} \quad (15)$$

which gives a linear force estimate on the order of  $F \approx 10^7 Nm^{-1}$  for the selected extreme physical/geometrical parameters. Note that the force drops rapidly as  $F \approx K^{-2}$ , when the number of coils is increased (Hoffman *et al.*, 2005).

#### *Detailed Magnetic Field Calculations*

There are several viable ways of calculating stationary magnetic fields created by a fixed, prescribed current distribution  $\vec{j}(\vec{r})$ :

- i. solving the Poisson equation for the vector-potential:  $\nabla^2 \vec{A} = \vec{j}, \vec{B} = \nabla \times \vec{A}$ ;
- ii. solving the set of Maxwell equations with zero initial EM-fields and currents, but  $\frac{d\vec{j}(\vec{r})}{dt} \neq 0$  until the currents are matched, and a steady-state regime is achieved;
- iii. direct calculation of the static magnetic field by using the Biot-Savart Law.

The first method is known to produce the smoothest fields. But it requires a spatial mesh, which is true for the second method as well. If the mesh is structured or uniform, both methods achieve poor accuracy in the coil vicinity, where the gradients are the highest. The only possibility to overcome this problem is to use non-uniform meshes. In general it leads to the utilization of the so-called unstructured grids and corresponding methods, characterized with a high level of numerical complexity (Hoffman *et al.*, 2005).

## Results

The simulation results are as follows:

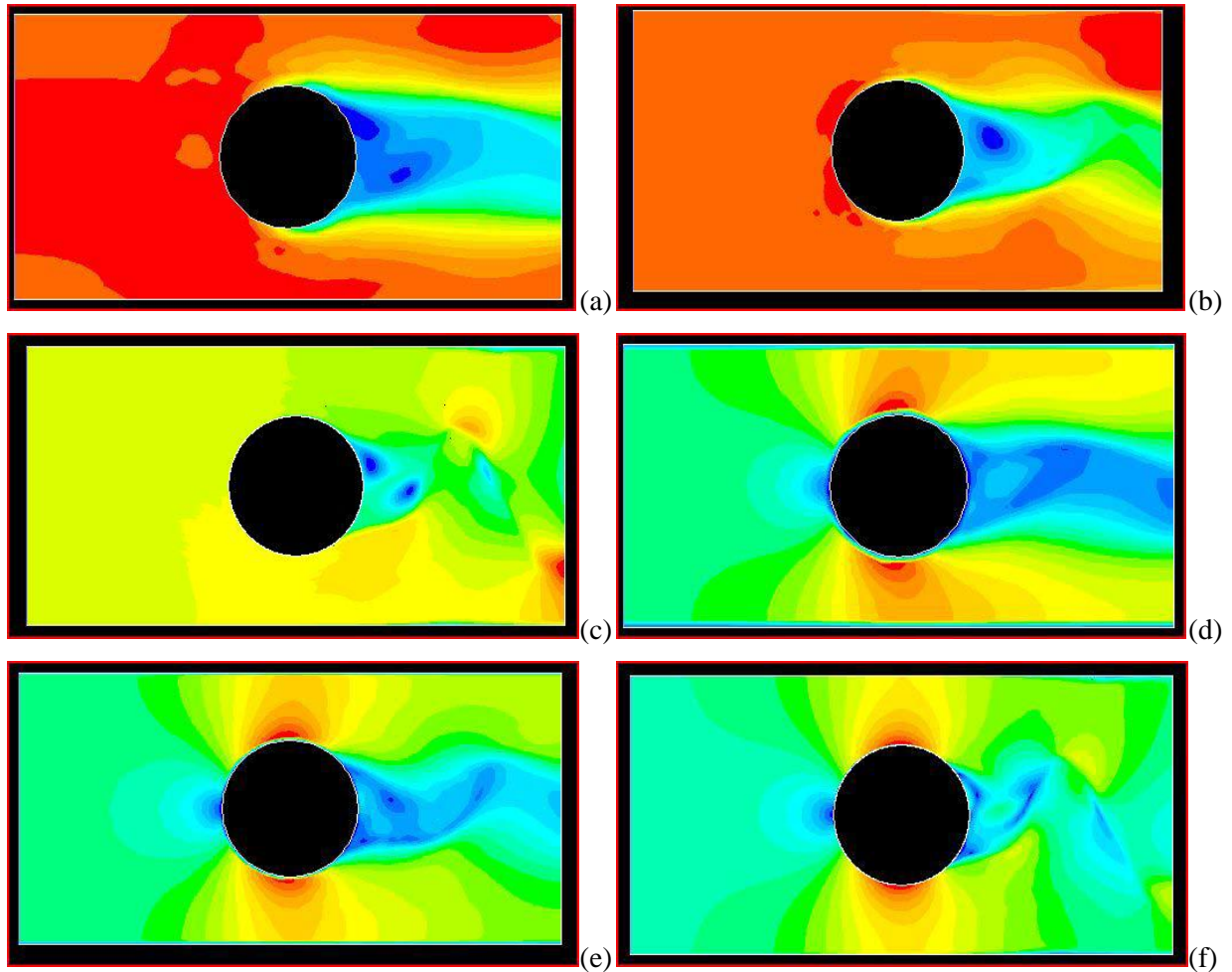


Figure 10: Simulated pressure at (a) 0.1 Resolution (b) 0.05 Resolution (c) 0.01 Resolution; and simulated velocity at (d) 0.1 Resolution (e) 0.05 Resolution (f) 0.01 Resolution.

The results from ANSYS work bench are given as follows:

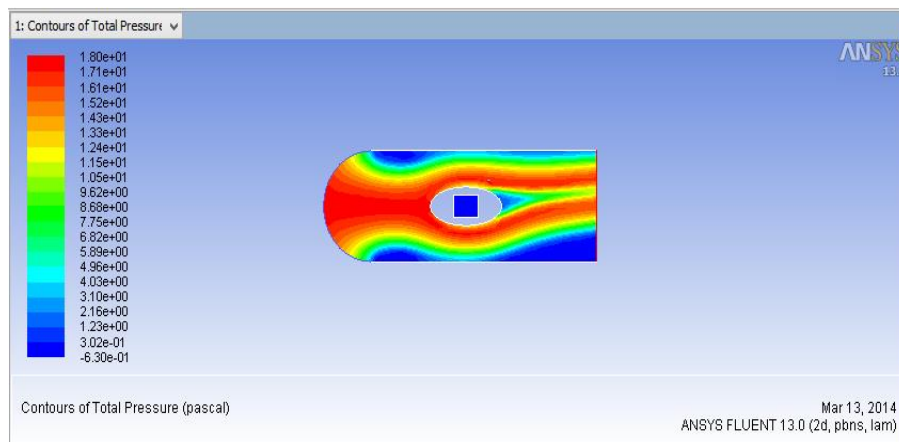


Figure 11: The contours of total pressure



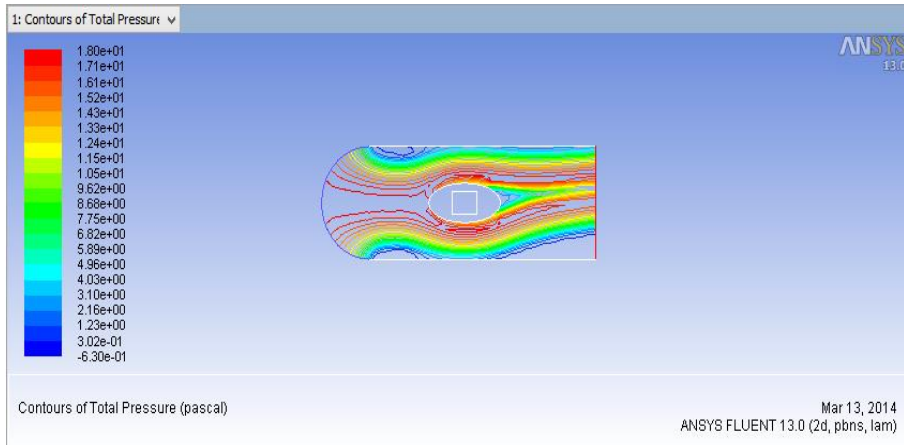


Figure 12: The contours of total pressure without filled checked.

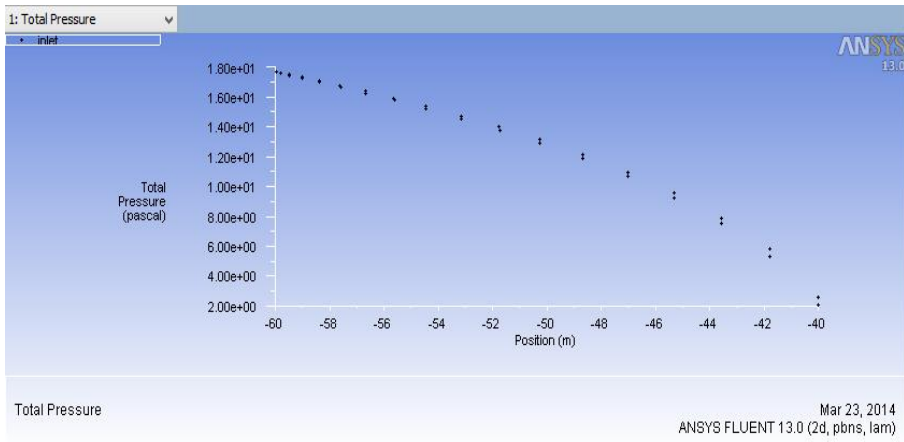


Figure 13: Total pressure simulation

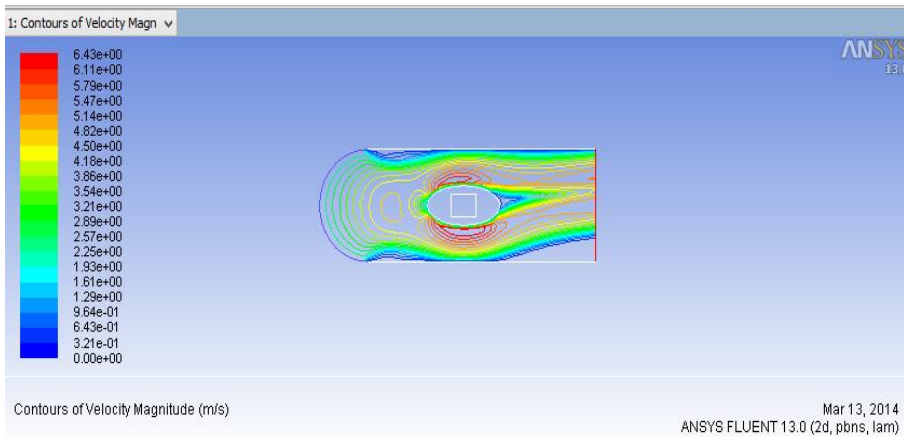


Figure 14: The contours of velocity magnitude

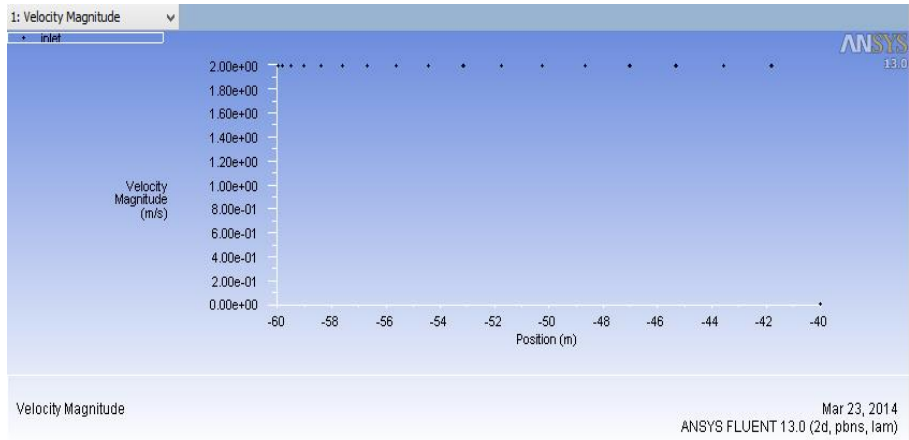


Figure 15: Velocity Magnitude

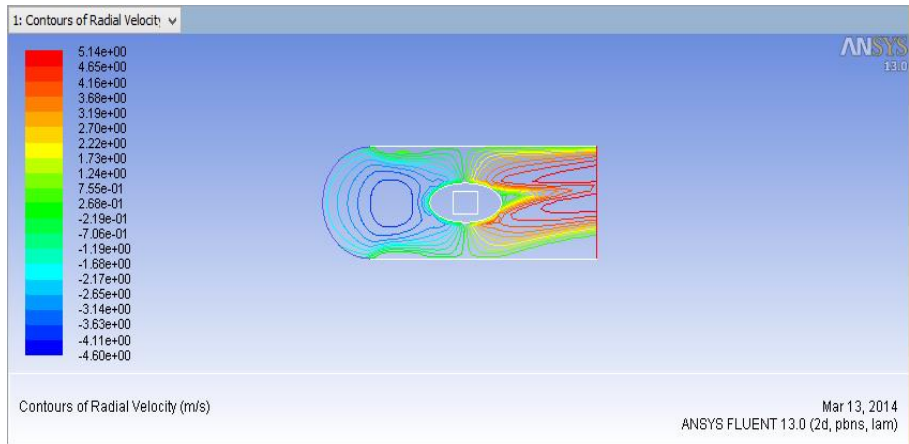


Figure 16: The contours of radial velocity

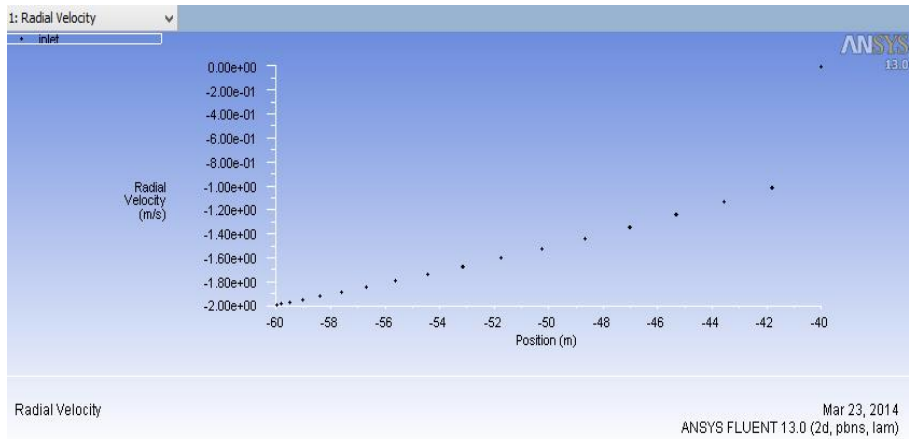


Figure 17: Radial velocity simulation

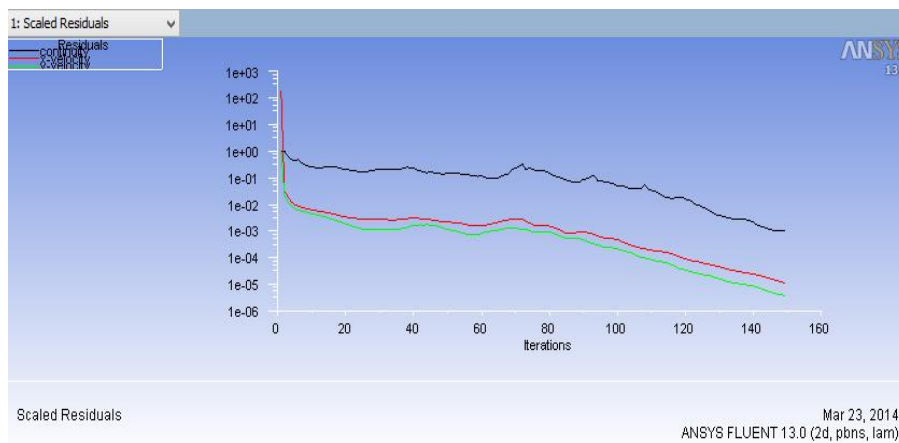


Figure 18: Scaled residuals

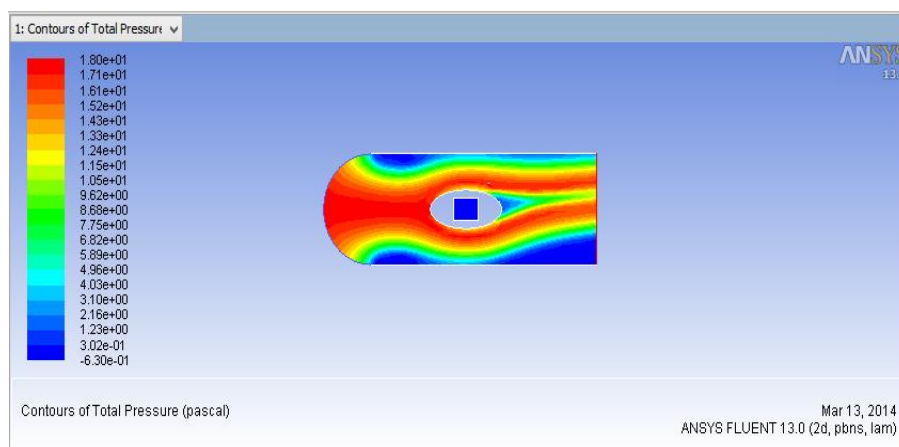


Figure 19: The Contours of total pressure

## Discussions

The ellipse, the cube and the semi-circle in Figure 19 were represented as the magnetic shield, the satellite and the sun respectively. As solar flares occur, the magnetic energy that is built up in the solar atmosphere is suddenly released. Radiation is emitted across virtually the entire electromagnetic spectrum, from radio waves at the long wave-length end, through optical emission to x-rays and gamma rays at the short wavelength end.

As the magnetic field from the solar flares approaches the satellite (cube), the ship-board coils

always have its magnetic field created around the satellite (ellipse) and thus deflecting charged particles coming toward the satellite. This concept of shielding a satellite from effect of solar flares is called Magnetic Shielding as illustrated in figures 10 to 18. Several sequences of how the event took place for a particular time interval can be created as animations. These animations could help in accessing how satellite construction can be optimized for minimum interaction with energetic solar particles.

## Conclusion

Having analyzed the harms that can be caused by solar flares, the simulations performed in this study show that if a built-in-detector can be constructed to sense the magnetic radiation of the solar flares then, the superconducting coil/toroid surrounding the components on board in the satellite will create a magnetic field that will shield the satellite components from direct effect of solar flares. From

the result of the simulations, it is recommended that a good detector should be constructed, and magnetic shielding method should be taken into consideration to shield any satellites launched to space from the hazardous solar flares. While this is done, the varying sunspots cycle also have been taken into consideration.

## References

- Harsh, B. and Ananna, B. (2012). "Effect of Solar Flares on Communication" *IRACST – International Journal of Computer Networks and Wireless Communications (IJCNWC)*, ISSN: 2250-3501 Vol. 2, No. 1, 2012
- Hoffman, J., Fisher, P. and Batishchev, O. (2005). "Use of Superconducting Magnet Technology for Astronaut Radiation Protection" Final Report for NIAC Phase 1 Contract CP 04-01. pp 8, 18-20.
- [http://en.wikipedia.org/wiki/Solar\\_flare](http://en.wikipedia.org/wiki/Solar_flare) [cited 29/01/13]
- <http://hesperia.gsfc.nasa.gov/sftheory/flare.htm> [cited 28/01/13]
- <http://www.wired.co.uk/news/archive/2010-06/15/how-to-survive-a-solar-storm> [cited 18/05/13]
- <http://www.todayshomeowner.com/how-to-protect-your-home-from-solar-flares-and-solar-storms/>[cited 18/05/13]
- <http://www.mnn.com/earth-matters/space/stories/solar-flare-could-disrupt-earth-s-satellite-communications> [cited 29/01/13]
- <http://www.wpi.edu/Pubs/E-project/Available/E-project121509172041/unrestricted/mqp.pdf> [cited 14/02/14]
- James A. Marusek. (2007). "Solar Storm Threat Analysis" Report on Impact 2007 Bloomfield indiana 47424. pp 1-4.
- McCracken, K.G., D.F. Smart, M.A. Shea, and G.A.M. Dreschhoff (2001) "400 years of large fluence solar proton events", Proceedings of 27th ICRC at Hamburg, 8, 2001, pp 3209-3212.
- Yan C. Wong. (1991). "Satellite Anomalies and Electrostatic Surface Discharges" Study from Naval Postgraduate School, Monterey, California. pp1-3.